Engineering Structures 293 (2023) 116658

Contents lists available at ScienceDirect

Engineering Structures

journal homepage: www.elsevier.com/locate/engstruct

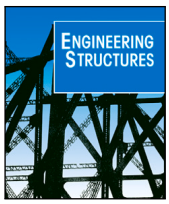

A numerical method for the funicular analysis of masonry vaults accounting for stereotomy, finite strength and finite friction

Danila Aita, Matteo Bruggi *

Department of Civil and Environmental Engineering, Politecnico di Milano, 20133, Milano, Italy

ARTICLE INFO

Keywords:
Funicular analysis
Masonry vaults
Masonry domes
Stereotomy
Finite friction
Finite strength
Mathematical programming

ABSTRACT

The funicular analysis of curved masonry structures is addressed, considering the stereotomy of the voussoirs, a limited compressive strength, and a limited friction coefficient. The force density method is used to handle the equilibrium of the loaded nodes of the network, whose vertices lie along vertical lines passing through the centroids of the blocks. For the resulting grid with fixed plan projection, the minimization of the horizontal thrusts is formulated in terms of the height of the restrained nodes and of any set of independent force densities. Anti-funicular networks are sought by enforcing compression-only branches of the network. Local constraints are stated at each joint addressing the hypothesis of a limited compressive strength and a finite value of the friction coefficient between two adjacent voussoirs. To enforce no-tension blocks, lower and upper bounds for the vertical coordinates of the unrestrained vertices of the network are prescribed, as well. Sequential convex programming is used to solve the arising multi-constrained minimization problem. The algorithm, which can handle networks with general topology, is assessed by comparisons with results achieved with the Durand–Claye method, a semi-analytical method for the equilibrium analysis of symmetric masonry arches and domes that accounts for the limited compressive strength of masonry, the friction coefficient and the stereotomy of the voussoirs. Numerical examples concern arches, domes and a cloister vault, considering varying mechanical parameters.

1. Introduction

The current study addresses a topical research problem in modern structural mechanics, namely the investigation of the structural response of unreinforced masonry arches, vaulted structures and domes. With reference to this issue, this contribution aims at extending the funicular analysis method to evaluate the mechanical response of structural elements of any complex shape, taking into account the geometry of the blocks and the mechanical properties of the joints.

The theoretical background is based on those methods which, re-evaluating pre-elastic theories [1], have framed the study of the mechanical behaviour of masonry structures in the context of limit analysis. As is well known, Heyman [2], by starting from insights in [3], transferred the philosophy of plastic theory from steel structures to the stone skeleton, and formulated his safe theorem for masonry arches by assuming the following hypotheses: the arch is made of perfectly rigid voussoirs having infinite compressive strength; there is no sliding between the voussoirs (i.e. the friction coefficient can be considered infinite); the tensile strength is nil. According to these hypotheses the research of the collapse condition can be determined either through the lower-bound or the upper-bound theorem of limit analysis, since the normality law holds between statically admissible stress states and the associated flow rule for the displacement field. A number of studies have re-worked historical methods based on the lower bound theorem of limit analysis; among them the thrust line method has been exploited e.g. in [4]. The modern re-visitation of the inversed catenary concept [5], as well as the progresses of the thrust line method in terms of graphical statics [6], have allowed the development of computerized methods aimed at drawing the funicular polygon corresponding to the actual loads for the assessment of masonry structures with complex geometry. The funicular analysis approach is one of the general methods arising from the context described above. A review of the state of the art on the scientific literature related to this method is beyond the scope of this contribution. The interested reader can refer e.g. to [7,8]. Without claiming completeness, however, we briefly recall some contributions that are significant for framing the research object of this paper. The funicular analysis method was firstly introduced in [9], suggesting a technique able to model the principal stresses in a masonry vault as a discrete network of forces. The forces meeting at each node must be in equilibrium with the forces applied at that node. By assuming that the forces in the network cannot be tensile, the nodes must lie within

* Corresponding author.
E-mail address: matteo.bruggi@polimi.it (M. Bruggi).

https://doi.org/10.1016/j.engstruct.2023.116658
Received 14 April 2023; Received in revised form 19 June 2023; Accepted 23 July 2023
Available online 3 August 2023
0141-0296/© 2023 The Author(s). Published by Elsevier Ltd. This is an open access article under the CC BY license (http://creativecommons.org/licenses/by/4.0/).

the thickness of the vault. This approach has been developed by various scholars, see in particular the contribution in [10] and the recent developments in [11,12]. Some outcomes provided in [13] have contributed to improve the method by exploiting the force density concept for linearizing the equilibrium of the nodes of a general network. In [14] an effective technique of matrix algebra is implemented to detect the dependent and independent sets of force densities that arise in the case of fixed horizontal projection of the network. The thrust network analysis approach has also led to interesting re-interpretations in terms of truss-like stress paths derived from Airy stress functions [15–17] or singular stress fields based on the Airy function [18–21].

As regards Heyman's hypotheses, which are usually adopted in the context of thrust network analysis, it should be noted that crushing and sliding can occur in real masonry structures. Neglecting the possibility of these events could lead to an overestimation of the collapse load, or result in unsafe solutions. Furthermore, the equilibrium of masonry structures is influenced by the stereotomy of the voussoirs, see in particular [22,23]. This is the starting point for the advances proposed in the current paper, where the problem is formulated within the framework of multi-constrained optimization. The outcome is a method of funicular analysis, introducing restrictions related to the compressive strength of masonry and assuming a limited finite friction at the interfaces of each block. This implies that the stereotomy of the voussoirs is taken into account. As for the mathematical formalization of the problem, reference is made to the contribution in [24], of which the algorithm proposed in the current paper can be viewed as an extension. The procedure consists in fixing the plan projection of the structural grid. Then, the equilibrium equations of the loaded nodes are written in terms of any independent set of force densities, along with the height of the restrained nodes. To achieve anti-funicular networks, compression-only constraints are implemented for the force densities. To guarantee that the blocks are not subjected to tensile stresses, lower and upper bounds for the vertical coordinates of the unrestrained vertices of the network are imposed. Furthermore, local constraints are enforced at each joint with the aim to take into account the effects of the limited compressive strength, as well as the limited friction coefficient. The arising multi-constrained minimization problem is solved through methods of sequential convex programming, which were originally conceived to tackle problems of structural optimization including multiple sets of local enforcements. The method is validated by considering some benchmark case studies. The results are compared with those obtained by means of a classical semi-analytical graphical method, originally devised by the French scholar Durand–Claye [25]. A re-visited version of this method, formulated in [26–28] in terms of the static theorem of limit analysis, is exploited and further developed in order to determine the complete set of admissible solutions with respect to both the equilibrium conditions, the strength requirements of the material, and the finite friction coefficient.

Before proceeding further, some remarks on the hypotheses adopted to describe the behaviour of masonry are necessary to rigorously setting the problem from a mechanical point of view. The introduction of a limited compressive strength enriches Heyman's assumptions imposing a more restrictive condition on the stresses, according to which the thrust line must pass inside each joint. Such an assumption allows to solve the equilibrium problem in terms of the lower bound theorem of limit analysis. On the contrary, considering the presence of finite friction opens a very subtle question from the mechanical point of view. If friction is finite, any two adjacent voussoirs may slide with respect to one another, and the normality rule does not hold. The material has therefore a non-standard plastic behaviour and is governed by a non-associated flow rule. As first observed by Drucker [29], the case of finite friction coefficient requires investigating if the system is "still intelligent enough to distribute the stress to avoid collapse", as well as assessing if the theorems of limit analysis are still valid. Since extreme theorems cannot be applied to limit analysis of non-standard materials, some scholars conceived modified bounding criteria. Radenkovic [30] demonstrates two theorems which allow for re-interpreting the results of limit analysis when the normality rule is not respected. The contribution in [31] is aimed at constructing a non-associated plastic potential to obtain a sufficient condition of uniqueness. The theoretical background on this subject is exploited by several scholars, see e.g. [32,33], to develop computational strategies for limit analysis of masonry structures. In [34] a mathematical programming procedure is proposed, based on non-linear and non-convex optimization, to determine the minimum of a class of statically and kinematically admissible load factors. This approach is implemented by [35,36] for non-standard limit analysis of block masonry structures. In [37] this issue is considered as a special constrained optimization problem. To the aims of this research, reference is made to some studies which identify, within non-standard limit analysis, some classes of problems for which the uniqueness of the solution is guaranteed, as well as the possibility of determining safe stress states. In [38] it is proved that the collapse of masonry arches with symmetric loading and geometry belongs to such class of problems. In [39] these results are extended to axisymmetric masonry domes, by proposing a lower-bound computer method able to take into account the effect of different friction coefficients at the joints. As regards the examination of more complex cases where non-standard behaviour occurs, the current study refers to the contribution by [32], where the yield surface for an assembly of blocks with Coulomb friction is analysed and a condition on stress-resultant systems is formulated to conclude about the safety of the achieved statically admissible solutions. Some further remarks on Coulomb friction as regards the equilibrium of masonry arches are given in [40,41]. The interest in non-standard limit analysis of masonry arches is testified also nowadays by some recent works focused on different aspects related to the presence of friction between the voussoirs, see e.g. [42–46]. It is interesting to observe that the method proposed in this paper, by considering the influence of both the shape of the voussoirs and restrictions on the material behaviour at the joints, can also offer interesting points of contact with the procedure adopted in [42]. In the latter contribution, the discrete element method is employed to investigate the mechanical behaviour of masonry oval domes with finite friction.

In the remainder of this paper, Section 2 recalls fundamentals of the force density method for networks with fixed plan projection. Section 3 presents the minimization problem, with focus on the constraints enforced at the joints between adjacent voussoirs, whereas Section 4 introduces the Durand–Claye method for the equilibrium of arches and domes. In Section 5 the performed simulations are reported, including comparisons of the results achieved by the proposed numerical method with those found through the aforementioned semi-analytical graphical approach. Section 6 concludes the paper, summarizing the outcome of this work and outlining the ongoing research.

2. Force density method for networks having fixed plan projection

The equilibrium of funicular networks is handled by means of the "force density method" [13]. A spatial network is made of $n_s = n + n_f$ nodes and m branches, the latter undergoing axial forces only. Denoting by x, y, and z the axes of the Cartesian reference system with origin O, the vectors $\mathbf{x}_s$, $\mathbf{y}_s$, $\mathbf{z}_s$ gather the coordinates of the n_s nodes: $\mathbf{x}$, $\mathbf{y}$, $\mathbf{z}$ refer to the n unrestrained nodes, where external loads are applied; $\mathbf{x}_f$, $\mathbf{y}_f$, $\mathbf{z}_f$ address the n_f restrained nodes, where reactions arise. Upon introduction of the connectivity matrix $\mathbf{C}_s$, the vectors $\mathbf{u}$, $\mathbf{v}$, $\mathbf{w}$ collect the difference in the coordinates of the nodes at the ends of each branch along the axis x, y, z, respectively, i.e.:

$$\mathbf{u} = \mathbf{C}_s\mathbf{x}_s, \quad \mathbf{v} = \mathbf{C}_s\mathbf{y}_s, \quad \mathbf{w} = \mathbf{C}_s\mathbf{z}_s. \tag{1}$$

For instance, u_i is the difference in terms of the x coordinate between the nodes at the end of the i-th branch. The force densities vector $\mathbf{q} = \mathbf{L}^{-1}\mathbf{s}$ stores the ratio force to length for each branch of the network, being $\mathbf{s}$ the vector gathering the forces in the m branches, and $\mathbf{L} = \mathrm{diag}(\mathbf{l})$ a square matrix collecting, along its diagonal, the

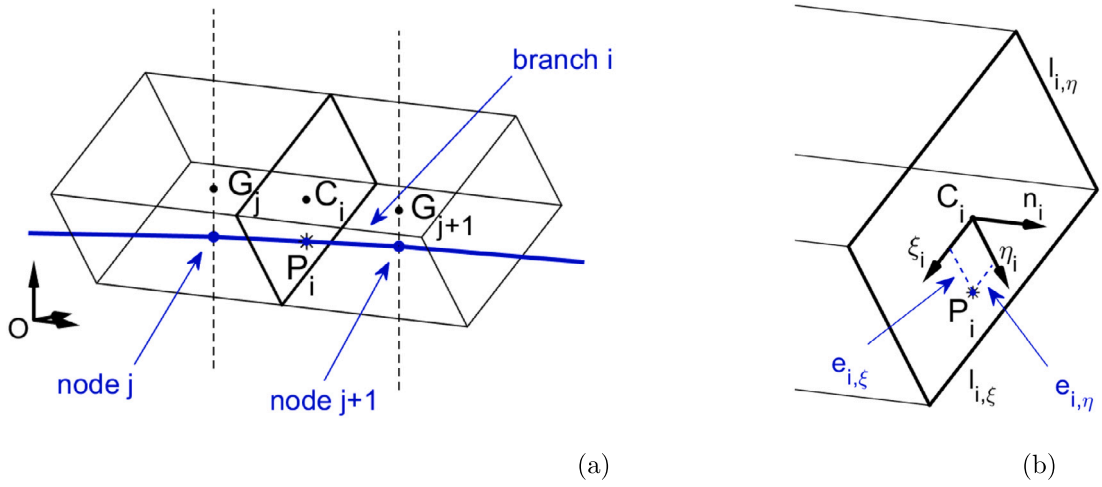

Fig. 1. The i-th joint between two adjacent voussoirs: view of the blocks (a); close-up of the joint (b).

length of the branches $l_i = \sqrt{u_i^2 + v_i^2 + w_i^2}$. Point loads are prescribed at the unrestrained nodes through vectors $\mathbf{p}_x$, $\mathbf{p}_y$, $\mathbf{p}_z$, which define the components of the nodal forces along the Cartesian axes. The introduction of the force densities allows for writing the equilibrium of the loaded nodes by means of linear equations which are uncoupled in the three spatial directions. It is assumed that the topology of the network is such that it can withstand the prescribed loads. As discussed in [14,47–50], for networks with fixed plan projection, the horizontal equilibrium of the unrestrained nodes reads:

$$\begin{bmatrix} \mathbf{C}^T \mathrm{diag}(\mathbf{C}_s \mathbf{x}_{s0}) \\ \mathbf{C}^T \mathrm{diag}(\mathbf{C}_s \mathbf{y}_{s0}) \end{bmatrix} \mathbf{q} = \begin{bmatrix} \mathbf{p}_x \\ \mathbf{p}_y \end{bmatrix}, \tag{2}$$

where the vectors $\mathbf{x}_{s0}$ and $\mathbf{y}_{s0}$ store the prescribed and fixed x and y coordinates of the nodes, respectively, and $\mathbf{C}$ is the subset of $\mathbf{C}_s$ referring to the unrestrained nodes. Eq. (2) implies that a set of $m - r$ independent force densities $\overline{\mathbf{q}}$ exists, being r the rank of the coefficient matrix. The r dependent force densities $\widetilde{\mathbf{q}}$ may be re-written as:

$$\widetilde{\mathbf{q}} = \mathbf{B}\overline{\mathbf{q}} + \mathbf{d}, \tag{3}$$

where $\mathbf{B}$ and $\mathbf{d}$ are matrices whose constant entries can be derived by applying Gauss–Jordan elimination to Eq. (2), see [51]. Upon introduction of $\mathbf{Q} = \mathrm{diag}(\mathbf{q})$, the vertical coordinates of the unrestrained nodes can be found by solving the equilibrium along the z axis, i.e.:

$$\mathbf{C}^T\mathbf{Q}\mathbf{C}\mathbf{z} + \mathbf{C}^T\mathbf{Q}\mathbf{C}_f\mathbf{z}_f = \mathbf{p}_z, \tag{4}$$

where $\mathbf{C}_f$ is the subset of $\mathbf{C}_s$ referring to the restrained nodes.

For simplicity, the adopted approach has been presented considering only unrestrained nodes, along with fully restrained ones, see [13]. Partially restrained nodes can be tackled upon introduction of suitable subsets of the connectivity matrix: $\mathbf{C}_{fx}$, $\mathbf{C}_{fy}$ and $\mathbf{C}_{fz}$ denote the subsets of $\mathbf{C}_s$ referring to the nodes with restraints along x, y and z, respectively, whereas $\mathbf{C}_x$, $\mathbf{C}_y$ and $\mathbf{C}_z$ stand for their complementary subsets to $\mathbf{C}_s$. The horizontal equilibrium is given by Eq. (2), provided that $\mathbf{C}$ is replaced by $\mathbf{C}_x$ and $\mathbf{C}_y$ in the first and in the second row, respectively. Eq. (4) holds, if $\mathbf{C}$ is changed into $\mathbf{C}_z$, and $\mathbf{C}_f$ into $\mathbf{C}_{fz}$. In the latter equation, $\mathbf{z}_f$ refers to the nodes with restraints along z, while $\mathbf{z}$ is its complement to $\mathbf{z}_s$.

3. Funicular analysis with finite strength and finite friction

3.1. Forces and eccentricities at the joint between two adjacent voussoirs

In Fig. 1, the i-th branch of the network spans from the unrestrained node j to the node $j + 1$, crossing a (dry) joint between two adjacent voussoirs. The nodes j and $j + 1$ are located along vertical lines passing through the centre of gravity of the blocks, which are G_j, with coordinates $(x_{G_j}, y_{G_j}, z_{G_j})$, and G_{j+1}, respectively. Due to the assumption of networks with fixed plan projection, only the vertical coordinates z_j and z_{j+1} are allowed to change during the optimization.

In the implementation that follows it is assumed that the i-th joint can be handled as a rectangular section. The largest rectangle that may be inscribed in the original shape is adopted. The centroid C_i of the considered rectangular section has coordinates $(x_{C_i}, y_{C_i}, z_{C_i})$. Denoting by $\mathbf{e}_x$, $\mathbf{e}_y$, $\mathbf{e}_z$ a triplet of unit vectors aligned with x, y, z, respectively, the principal axes of inertia are given by $\boldsymbol{\xi}_i = \xi_{i,x}\,\mathbf{e}_x + \xi_{i,y}\,\mathbf{e}_y + \xi_{i,z}\,\mathbf{e}_z$ and $\boldsymbol{\eta}_i = \eta_{i,x}\,\mathbf{e}_x + \eta_{i,y}\,\mathbf{e}_y + \eta_{i,z}\,\mathbf{e}_z$, where $\xi_{i,x}$, $\xi_{i,y}$, $\xi_{i,z}$ and $\eta_{i,x}$, $\eta_{i,y}$, $\eta_{i,z}$ are the direction cosines. The size of the section is $l_{i,\xi} \times l_{i,\eta}$. The normal outgoing from the j-th voussoir is defined as $\mathbf{n}_i = n_{i,x}\,\mathbf{e}_x + n_{i,y}\,\mathbf{e}_y + n_{i,z}\,\mathbf{e}_z$, with $n_{i,x}$, $n_{i,y}$, $n_{i,z}$ direction cosines.

The force acting upon the j-th block, due to the entry s_i of the force vector $\mathbf{s}$, is:

$$\mathbf{F}_i = s_i \left(\frac{u_i}{l_i}\,\mathbf{e}_x + \frac{v_i}{l_i}\,\mathbf{e}_y + \frac{w_i}{l_i}\,\mathbf{e}_z \right) = q_i \left(u_i\,\mathbf{e}_x + v_i\,\mathbf{e}_y + w_i\,\mathbf{e}_z \right). \tag{5}$$

With respect to the plane of the i-th joint, i.e. that defined by the unit vectors $\boldsymbol{\xi}_i$ and $\boldsymbol{\eta}_i$, a normal and a shear component of $\mathbf{F}_i$ are introduced, $\mathbf{N}_i$ and $\mathbf{V}_i$ respectively. The magnitude of the normal component of the force may be computed by observing that:

$$N_i = \mathbf{F}_i \cdot \mathbf{n}_i = q_i \left(u_i\,n_{i,x} + v_i\,n_{i,y} + w_i\,n_{i,z} \right), \tag{6}$$

where a negative value of N_i stands for compression. Hence, the magnitude of the shear component may be found as the modulus of the vector difference $\mathbf{F}_i - \mathbf{N}_i$, i.e. $\mathbf{F}_i - N_i\mathbf{n}_i$, that implies:

$$V_i^2 = \left(q_i\,u_i - N_i\,n_{i,x} \right)^2 + \left(q_i\,v_i - N_i\,n_{i,y} \right)^2 + \left(q_i\,w_i - N_i\,n_{i,z} \right)^2. \tag{7}$$

The eccentricity of $\mathbf{N}_i$ with respect to $\boldsymbol{\xi}_i$ may be found by evaluating the moment of the normal component of the force about the same axis, $M_{i,\xi}$, scaled by N_i. Recalling that the shear component of the force does not provide any contribution to $M_{i,\xi}$, and denoting by $\mathbf{r}_i = (x_{sj} - x_{C_i})\,\mathbf{e}_x + (y_{sj} - y_{C_i})\,\mathbf{e}_y + (z_{sj} - z_{C_i})\,\mathbf{e}_z$ the vector drawn from C_i to the j-th node of the network, one has that $M_{i,\xi} = \boldsymbol{\xi}_i \cdot (\mathbf{r}_i \times \mathbf{F}_i)$. Hence:

$$e_{i,\xi} = \mathrm{abs}\left(\frac{M_{i,\xi}}{N_i} \right), \text{with } \frac{M_{i,\xi}}{N_i} = \\ = \frac{1}{u_i\,n_{i,x} + v_i\,n_{i,y} + w_i\,n_{i,z}} \begin{vmatrix} \xi_{i,x} & \xi_{i,y} & \xi_{i,z} \\ x_{sj} - x_{C_i} & y_{sj} - y_{C_i} & z_{sj} - z_{C_i} \\ u_i & v_i & w_i \end{vmatrix}, \tag{8}$$

where $\mathrm{abs}(\cdot)$ stands for the absolute value of a scalar argument and $|\cdot|$ for the determinant of a matrix argument. Analogously, the eccentricity

of $\mathbf{N}_i$ with respect to $\boldsymbol{\eta}_i$ may be found as:

$$e_{i,\eta} = \text{abs}\left(\frac{M_{i,\eta}}{N_i}\right), \text{with } \frac{M_{i,\eta}}{N_i} = \\ = \frac{1}{u_i\, n_{i,x} + v_i\, n_{i,y} + w_i\, n_{i,z}} \begin{vmatrix} \eta_{i,x} & \eta_{i,y} & \eta_{i,z} \\ x_{sj} - x_{C_i} & y_{sj} - y_{C_i} & z_{sj} - z_{C_i} \\ u_i & v_i & w_i \end{vmatrix}, \tag{9}$$

where $M_{i,\eta}$ stands for the moment of the force $\mathbf{F}_i$ about the same axis $\boldsymbol{\eta}_i$.

The above formulas do not change when the i-th branch of the network connects a restrained node with one of the unrestrained set, the latter lying along a vertical line passing through the centroid of a block at the boundary of the curved structure. The assessment of the joint crossed by the considered branch is performed looking at the relevant section of the voussoir. The ingoing normal is selected, instead of the outgoing one, if the first node of the branch is the restrained one.

3.2. A multi-constrained minimization problem for funicular networks of minimum thrust

The method herein proposed, framed in the theoretical context of limit analysis, investigates the existence of statically admissible funicular networks for the vault under examination. In particular, a multi-constrained minimization/maximization problem allows for identifying the funicular networks corresponding to the minimum and maximum thrust values. In order to validate the numerical procedure, a focus on determining networks of minimum thrust is provided in this section. It should be observed that such networks do not correspond to the "true" solution, but to one of the infinite statically admissible ones. It is worth mentioning that, under Heyman's hypotheses, masonry vaults often attain a state of minimum thrust after the onset of settlement at the supports, see e.g. [2,52]. In these cases the choice to minimize the thrust is also significant from a mechanical point of view. Aiming at minimizing the overall thrust, the following problem is considered:

$$\begin{cases} \min\limits_{\substack{\overline{\mathbf{q}}\le\mathbf{0} \\ \mathbf{z}_f^{\min}\le\mathbf{z}_f\le\mathbf{z}_f^{\max}}} & f = \sum\limits_h^{n_f}\left(R_{x\,h}^2 + R_{y\,h}^2\right) & \text{(a)} \\ \text{s.t.} & \widetilde{\mathbf{q}} = \mathbf{B}\overline{\mathbf{q}} + \mathbf{d}, & \text{(b)} \\ & \mathbf{C}^T\mathbf{Q}\mathbf{C}\mathbf{z} + \mathbf{C}^T\mathbf{Q}\mathbf{C}_f\mathbf{z}_f = \mathbf{p}_z, & \text{(c)} \\ & \widetilde{q}_k \le 0 \quad \text{for } k = 1...r, & \text{(d)} \\ & \frac{N_i}{\sigma_c\left(l_{i,\xi}-2e_{i,\eta}\right)\left(l_{i,\eta}-2e_{i,\xi}\right)} \le 1 \quad \text{for } i = 1...m, & \text{(e)} \\ & \frac{V_i^2}{\left(N_i\tan\psi\right)^2} \le 1 \quad \text{for } i = 1...m, & \text{(f)} \\ & z_j(\overline{\mathbf{q}}, \mathbf{z}_f) \ge z_j^{\min} \quad \text{for } j = 1...n, & \text{(g)} \\ & z_j(\overline{\mathbf{q}}, \mathbf{z}_f) \le z_j^{\max} \quad \text{for } j = 1...n, & \text{(h)} \end{cases} \tag{10}$$

where the vector storing the components of the reactions along the x and y direction, $\mathbf{R}_x$ and $\mathbf{R}_y$ respectively, can be computed as $\mathbf{R}_x = \mathbf{C}_f^T\text{diag}(\mathbf{C}_s\mathbf{x}_{s0})\mathbf{q}$ and $\mathbf{R}_y = \mathbf{C}_f^T\text{diag}(\mathbf{C}_s\mathbf{y}_{s0})\mathbf{q}$, see e.g. [24]. The minimization unknowns consist of any reduced set of independent force densities $\overline{\mathbf{q}}$ and of the vertical coordinates of the restrained nodes $\mathbf{z}_f$. The dependent force densities $\widetilde{\mathbf{q}}$ are recovered from the independent set $\overline{\mathbf{q}}$ by means of Eq. (10)-(b). Eq. (10)-(c) is the equilibrium of the unrestrained nodes in the vertical direction, which allows for computing $\mathbf{z}$. Side constraints are used to prevent the arising of any positive independent force density and to prescribe lower and upper bounds to the vertical coordinates of the n_f restrained nodes, see vectors $\mathbf{z}_f^{\min}$ and $\mathbf{z}_f^{\max}$, respectively. Depending on the connectivity of the spatial grid, the former condition may not be sufficient to ensure the achievement of anti-funicular networks, see [13]. To overcome this issue, local constraints on the set of the r dependent force densities are implemented in Eq. (10)-(d). Denoting by $\sigma_c \le 0$ the strength in compression, Eq. (10)-(e) consists of a set of local constraints that avoid crushing at each joint, by imposing a finite compressive strength and a nil tensile strength. A constant distribution of compressive stress is assumed to arise in a limited portion of the section of the i-th joint, i.e. the area with size $\left(l_{i,\xi} - 2e_{i,\eta}\right)\times\left(l_{i,\eta} - 2e_{i,\xi}\right)$, to withstand the eccentric axial force N_i. The adopted strength criterion is commonly used in the engineering practice, see, for instance, the ultimate limit state design of shallow foundations. When $e_{i,\xi} = 0$, or $e_{i,\eta} = 0$, it reduces to the well-known criterion for $M_{i,\eta}$ and N_i only, or $M_{i,\xi}$ and N_i only, as discussed e.g. in [22,26]. Upon introduction of the friction angle ψ, the set of local enforcements in Eq. (10)-(f) prevents the attainment of a limit condition at the i-th joint, by imposing that the ratio V_i to N_i must obey the Coulomb's law [1]. Finally, Eqs. (10)-(g) and (10)-(h) are used to prevent the occurrence of tensile stresses in the voussoirs, by enforcing lower and upper bounds to the vertical coordinates of the n unrestrained nodes. Indeed, $z_j^{\min}$ and $z_j^{\max}$, are, respectively, the minimum and the maximum value of the vertical coordinate that the j-th node may assume without exiting the voussoir. By using $\sigma_c \to -\infty$ in Eq. (10)-(e) and neglecting Eq. (10)-(f), the formulation in Eq. (10) retrieves networks of minimum thrust that comply with Heyman's assumptions. For finite values of σ_c and $\tan\psi$, the assumption of infinite strength and no-sliding are removed at all joints. In the context of limit analysis it may be useful to study the range of admissible solutions, looking for both the minimum and maximum thrust. Networks of maximum thrust can be retrieved through the minimization problem in Eq. (10) by using $-f$ as objective function.

It must be remarked that Eq. (10) implements a method of funicular analysis, meaning that equilibrium is enforced at the nodes only. Assuming that each voussoir corresponds to a vertex whose position can vary only along the line of action of the resultant of the external forces (herein self-weight acting as a vertical force through the centroid), any feasible solution of Eq. (10) retrieves equilibrium of the rigid blocks. At the i-th rectangular joint, strength constraints are enforced on the limit bending moment, accounting for $\mathbf{N}_i$, $e_{i,\xi}$ and $e_{i,\eta}$, see Eq. (10)-(e), whereas the strength/friction constraints on the magnitude of the twisting moment resulting from the eccentricity of $\mathbf{V}_i$ are implicitly disregarded, see Eq. (10)-(f). This simplification allows for a direct comparison of the achieved numerical results with respect to those found through the Durand–Claye method, addressing symmetric structures that are symmetrically loaded. To tackle more general cases, Eq. (10) can be straightforwardly endowed with constraints related to the torsional capacity of the frictional interfaces, either including additional constraints, see e.g. [35], or replacing both Eq. (10)-(e) and Eq. (10)-(f) with limit functions accounting for interactions of torsion strength with bending moments and shear forces, see in particular the piece-wise linear approximation for rectangular interfaces proposed in [53].

3.3. Numerical details

As investigated in [24], Eq. (10) can be efficiently tackled through techniques of sequential convex programming that were originally conceived to handle problems of size optimization with multiple sets of local enforcements, see also the application in [54]. Due to its effectiveness in the solution of stress-based problems of topology optimization, see e.g. [55–59], the gradient-based Method of Moving Asymptotes (MMA) [60] is herein adopted. The sensitivity information is provided at each iteration. The gradient of $\mathbf{q}$ and $\mathbf{z}$ with respect to both sets of minimization unknowns $\overline{\mathbf{q}}$ and $\mathbf{z}_f$ can be computed by differentiation of the equilibrium equations following [50]. Once these are available, the chain rule allows to complete the task. When differentiating the relations in Eq. (1), the assumption of grids with fixed plan projection implies that:

$$\frac{\partial\mathbf{w}}{\partial\overline{q}_k} = \mathbf{C}\frac{\partial\mathbf{z}}{\partial\overline{q}_k}, \qquad \frac{\partial\mathbf{w}}{\partial z_{f\,h}} = \mathbf{C}_s\frac{\partial\mathbf{z}_s}{\partial z_{f\,h}} = \mathbf{C}\frac{\partial\mathbf{z}}{\partial z_{f\,h}} + \mathbf{C}_f\frac{\partial\mathbf{z_f}}{\partial z_{f\,h}}. \tag{11}$$

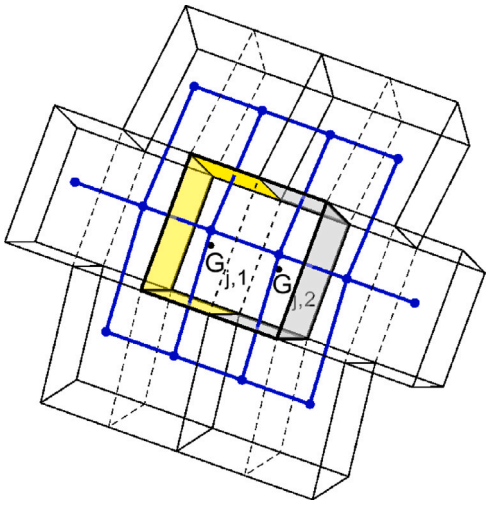

Fig. 2. Modelling of staggered masonry: the j-th voussoir is split into two sub-blocks, thus defining a pair of nodes of the funicular network (vertices and branches in blue); only the coloured sections are accounted as joints. (For interpretation of the references to colour in this figure legend, the reader is referred to the web version of this article.)

It must be also remarked that the constraint in Eq. (10)-(e) is non-differentiable when the eccentricities $e_{i,\xi}$ and $e_{i,\eta}$ are equal to zero, see Eqs. (8) and (9). To overcome this issue, the absolute value of the argument a, which is abs(a), is replaced with an approximation whose lower bound is the absolute value itself [61]:

$$a\,\mathrm{erf}\left(\frac{a}{\sqrt{2}\beta}\right)+\sqrt{\frac{2}{\pi}}\beta\exp\left(-\frac{a^2}{2\beta^2}\right), \tag{12}$$

where erf is the error function and $\beta = 0.05\min\left(l_{i,\xi}, l_{i,\eta}\right)$. The convolution operator introduces a minor bias around $a = 0$, i.e. for $e_{i,\xi} \to 0$ and $e_{i,\eta} \to 0$, while providing the required differentiability.

The enforcement of the constraints in Eqs. (10)-(e) and (10)-(f) can be conveniently restricted, if needed, to a subset of joints (and related network branches). In this regard, the strategy adopted to model staggered joints is exemplified in Fig. 2 . The j-th voussoir is split into two sub-blocks, thus defining a pair of nodes of the funicular network which can be connected to those representing the staggered blocks around. Only the sections connecting the j-th voussoir to its surroundings are accounted as joints, meaning that Eqs. (10)-(e) and (10)-(f) are disregarded at the inner interface between the two sub-blocks making the voussoir. The same splitting technique may be used to address voussoirs with complex shapes, see e.g. the blocks lying at the intersection of the four lunes in the cloister vault of Section 5.3. When no splitting is operated, each node of the network has a fixed plan projection corresponding to the horizontal coordinates of the centroid of the relevant block. This means that the topology of the network only depends on the connectivity among nodes whose horizontal projection is given. When sub-blocks are used, a number of different voussoir partitions can be adopted, thus allowing for additional degrees of freedom in the definition of the network. This can be exploited to create a correspondence between the geometry/layout of the blocks and the branches of the grid, by searching for the arising of networks that are consistent with the expected load path. In this regard, reference is also made to [22], where new equilibrium states are investigated considering networks where all the forces applied to one block do not intersect in the same point.

It is finally pointed out that Eq. (10) does not retrieve a collapse load, but searches among possible equilibrium states under a given loading condition, herein self-weight. A comparison with classical block methods for the limit analysis of masonry structures, see Section 1, can be done in terms of admissible equilibrium states. When the forces applied to each block, both the external ones and the reactions due to the adjacent voussoirs, are concurrent, the approaches are equivalent. When sub-blocking is used, the equilibrium states allowed by the funicular approach here presented may be seen as a subset of those considered when adopting classical block methods. The number of parameters that are needed to handle the equilibrium are remarkably less when working with the proposed funicular approach.

4. The Durand–Claye method and its modern version

In view of the assessment of the implemented numerical method, a classical semi-analytical graphical approach, known as “stability area method”, is outlined. This method is based on the static theorem of limit analysis, and aims at determining the complete set of admissible solutions with respect to both the equilibrium conditions and the strength capacity of the material. Originally conceived for the analysis of symmetric masonry arches subject to symmetric vertical loads [25,62], this graphical procedure consists in drawing the so-called “area of stability”, i.e. the locus of points formed by the extremes of the vectors representing all the horizontal thrusts satisfying both the equilibrium conditions for the entire structure, and the strength limitations related to masonry. More precisely, the stability area A is a region plotted in the (f, e_0) plane, where f is the horizontal thrust acting at point P_0 of the vertical cross-section at the crown, while e_0 is the eccentricity of f with respect to the cross-section’s centre of gravity C_0. In Fig. 3(a) the stability area is represented as a green region, being the intersection between the rotational domain A^{rot} (the yellow region) and the sliding domain A^{sl} (the bright blue one). The stability area method was re-visited and re-formulated in [26,27], framing it within the theoretical background of limit analysis. An enhanced version of this method was proposed in [28] to evaluate the stability of masonry domes. The graphical procedure was translated in terms of internal forces, and computerized, by resulting to be an effective tool for assessing the stability of symmetric masonry arches and domes of revolutions, loaded symmetrically. By adopting the same notation used in Section 3, it should be observed that, for symmetric arches with symmetric loading, only the bending moment $M_{i,\xi}$ exists, see Fig. 3(b). By denoting as θ_i the colatitude of the i-th joint with respect to the z axis, the equilibrium conditions related to the portion of the arch comprised between the vertical section at the crown and the i-th joint allow for writing the formal expressions of the internal forces $M_{i,\xi}$ and N_i as $M_{i,\xi} = M_{i,\xi}(f, e_0, \theta_i)$ and $N_i = N_i(f, \theta_i)$, respectively, for any joint. At each joint i, the limit bending moment $M^{lim}_{i,\xi}$ and the shear capacity can be defined according to a given criterion. In the following, $M^{lim}_{i,\xi}$ corresponds to a constant distribution of the limit compressive stresses σ_c at the joint, with possible partialization of the cross-section due to the zero tensile strength. Hence, $M^{lim}_{i,\xi}$ is determined as a function of the normal force N_i, of the dimensions of the cross-section, $l_{i,\xi}$ and $l_{i,\eta}$, and of the masonry compressive strength, σ_c:

$$M^{lim}_{i,\xi} = \frac{N_i\left(N_i - l_{i,\xi}\, l_{i,\eta}\, \sigma_c\right)}{2\, l_{i,\xi}\, \sigma_c}. \tag{13}$$

This condition is fully equivalent to that used in Eq. (10)-(e) when $M_{i,\eta} = 0$. In Fig. 3, the red and blue curves in the (f, e_0) plane correspond to the attainment of $+M^{lim}_{i,\xi}$ and $-M^{lim}_{i,\xi}$ at the i-th joint, respectively. The shear capacity of the cross-section is obtained by assuming the existence of internal friction along the joints, see Eq. (10)-(f) with the Coulomb’s friction coefficient $\tan\psi$. The values of the crown thrust such that the shear force V_i attains its limit value are:

$$f_i^{sl\pm} = W_i \tan\left(\pi/2 - \theta_i \pm \psi\right), \tag{14}$$

where W_i is the weight of the arch’s portion comprised between the vertical section at the crown and the generic joint. At any given joint: (i) the inequalities $-M^{lim}_{i,\xi} \le M_{i,\xi} \le +M^{lim}_{i,\xi}$ implicitly define the region A^{rot}_i in the (f, e_0) plane, which corresponds to the rotational domain

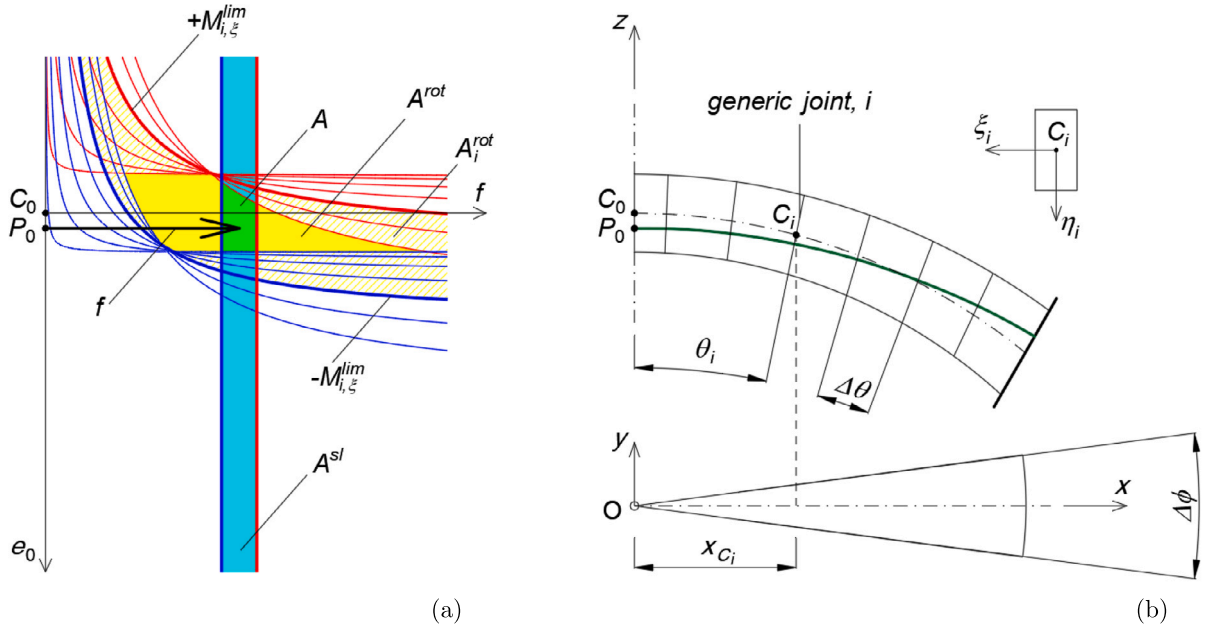

Fig. 3. The "stability area method": stability area A corresponding to all the admissible solutions in the (f, e_0) plane with respect to both the equilibrium conditions and the strength capacity of the material (a); thrust line corresponding to one of the infinite solutions (b).

related to the i-th joint; (ii) the conditions $f_i^{sl-} \le f_i \le f_i^{sl+}$ define the region A_i^{sl}, bounded by two vertical straight lines, which represents the sliding domain related to joint i. By repeating the procedure for all the joints and intersecting all the A_i^{rot} and A_i^{sl} regions, the rotational and sliding domains related to the entire arch are obtained, namely A^{rot} and A^{sl}. In Fig. 3(a) the former is plotted as a yellow area, whereas the latter is in bright blue. The area of stability A is obtained by intersecting the rotational and sliding domains A^{rot} and A^{sl}, i.e. the green area. When the stability area related to the entire arch is reduced to a single point (or a single segment), a limit condition is attained and the corresponding collapse mechanism is identified.

An extension of the method to masonry domes was proposed in [28], assuming an infinite friction coefficient as well as an infinite compressive strength. The dome is ideally sliced along the meridian planes by obtaining a series of "lunes". First, the stability area method is applied to the single lunes, conceived as independent arches. Then, it is observed that the limit condition identified by the vanishing of the stability area could not correspond to the activation of a collapse mechanism. To identify the limit condition, the possibility of activating a kinematically admissible collapse mechanism for the entire dome must be checked. It is also remarked that the presence of (statically indeterminate) hoop compressive forces in the upper portion of the dome could allow equilibrium although the area of stability related to the single lune is nil.

5. Numerical simulations

In Sections 5.1 and 5.2, the analysis of symmetric masonry arches and domes subjected to their self-weight, loaded symmetrically, is addressed. The stability area method is exploited to retrieve reference solutions for validation of the proposed numerical method. In Section 5.3 the equilibrium of a cloister vault is dealt with.

In case of infinite friction, the existence of any force network that is in equilibrium with the prescribed loads implies that the structure is safe for loading smaller than the given one, see the well-known lower-bound theorem of limit analysis. When a non-standard material is addressed, the normality of the flow rule is lost and the equilibrium is not enough to conclude about the safety of the structure [30]. As outlined in Section 1, a criterion to check the validity of any statically admissible solution is given in [32]. According to this contribution, safety can be questionable only if a set of self-equilibrating stress resultants exists, which respects all the constraints on the strength of the material. With reference to the implemented method of funicular analysis, this can be investigated by looking at the linear system that gathers Eqs. (2) and (4), assuming $\mathbf{p}_x = \mathbf{p}_y = \mathbf{p}_z = \mathbf{0}$. Non-trivial solutions did not arise for any of the structures analysed next.

All the achieved optimal solutions are fully feasible with respect to the set of the enforced constraints, meaning that no violation of any local enforcement was reported at convergence.

In all the pictures representing funicular networks, the symbols + and ∘ denote joint sections whose crossing branches activate a strength constraint. The former symbol is used when the point of intersection of the branch with the joint lies above the centroid of the section, the latter otherwise. The symbol × refers to any joint section whose crossing branch activates a friction constraint. The symbols ▵ and ▿ stand for points where a vertex of the network touches the extrados or the intrados of the existing envelope, respectively.

A material with specific weight $\gamma_m = 15$ kN/m^3 is assumed throughout the section.

5.1. Arch with non-conventional stereotomy

The arch with the profile represented in Fig. 4(a) is considered. The intrados lies along a circle with centre in $C_{in} = (0, 0, 0.5)$ m and radius $r_{in} = 6.0$ m. The extrados lies along a circle having centre in $C_{ex} = (0, 0, -0.5)$ m and radius $r_{ex} = 7.5$. One half of the angle of embracement reads $\alpha = 30°$. The out-of-plane thickness of the arch is $th = 0.5$ m. The arch is made of thirteen voussoirs, whose stereotomy is defined by radial lines originating from the point $C_{st} = (0, 0, -2.5)$ m. The funicular polygon has fifteen nodes ($n_s = 15$). Two external nodes are needed to define the branches crossing the boundaries of the arch. They are conventionally located along vertical lines passing through the outer edge of the boundary voussoirs. The nodes are restrained to the ground, thus generating two sets of reactions along the horizontal and the vertical direction ($n_f = 2$). Each one of the unrestrained inner nodes is loaded by the resultant of the self-weight of the relevant voussoir ($n = 13$). The resultant of the vertical forces reads 41.90 kN. One independent force density exists, meaning that the minimization

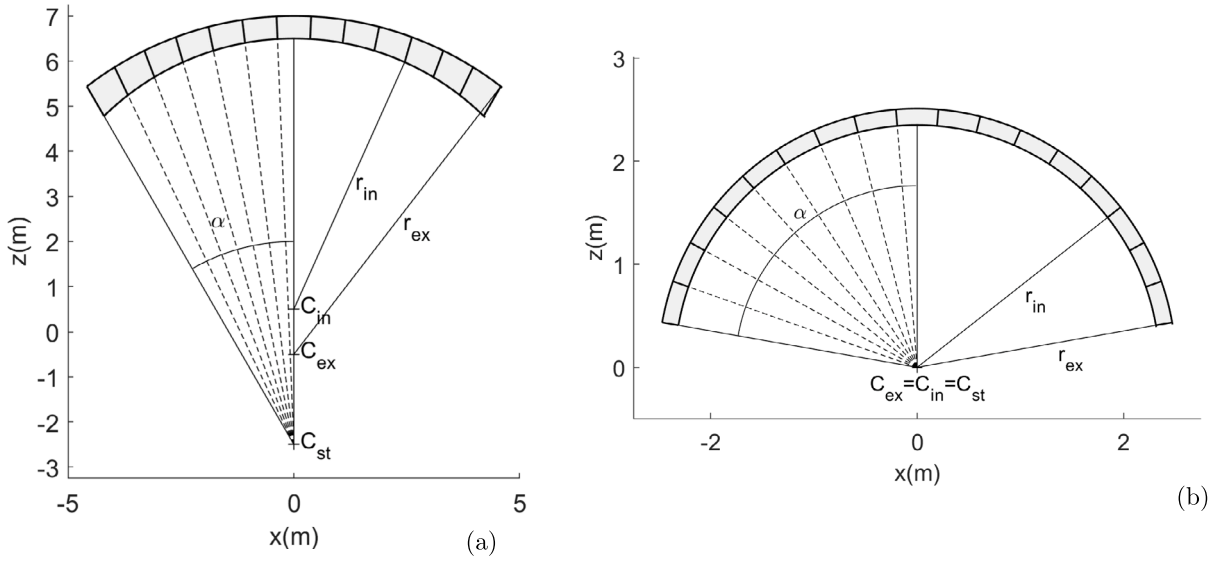

Fig. 4. Parametric geometry and stereotomy for the considered arcuated structures.

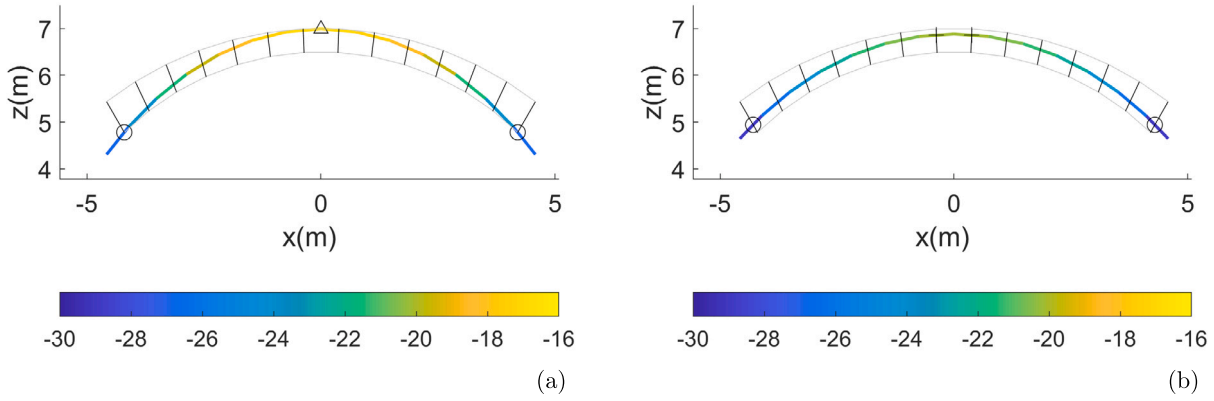

Fig. 5. Funicular polygons of minimum thrust for an arch with infinite friction: $\sigma_c = -1000$ MPa ($R_{xh} = 16.76$ kN) (a); $\sigma_c = -0.15$ MPa ($R_{xh} = 20.09$ kN) (b). The colours correspond to the value of the forces in the branches (in kN).

problem Eq. (10) is formulated in terms of three unknowns (one force density and the vertical coordinates of the two restrained nodes). Indeed, the funicular polygon of an arch is indeterminate to the third degree. The same initialization is used in all the simulations presented in Section 5. The starting guess for any independent force density is 50 kN/m, whereas entries of $\mathbf{z}_f$ are arbitrarily set to half of the maximum vertical coordinates of the vertices defining the geometry of the voussoirs along the boundary.

At first, the funicular polygon of minimum thrust is sought under Heyman's assumptions, i.e. looking at the case of infinite compressive strength and infinite friction resistance. The former requirement is approximated by using $\sigma_c = -1000$ MPa in Eq. (10)-(e), whereas the constraints in Eq. (10)-(f) are disregarded to meet the latter. The computed funicular polygon, along with the value of the element forces in its branches, gathered in $\mathbf{s}$, is reported in Fig. 5(a). Constraints of the type in Eq. (10)-(e) are active at both end joints, whereas a no-tension constraint is active for the block at the keystone, see Eq. (10)-(h). The funicular polygon spans from the lowest level of the abutments to become tangent to the extrados of the arch at the keystone, thus engaging the full envelope and getting the minimum horizontal reaction $R_{xh} = 16.76$ kN. A further simulation is performed, considering $\sigma_c = -0.15$ MPa in Eq. (10)-(e). The choice of such a low compressive strength value is related to the goal of validating the proposed procedure, without making explicit reference to any specific material. Incidentally, it can be recalled that Durand–Claye proposes a safety coefficient to evaluate the stability of masonry arches (in the hypothesis of an infinite friction coefficient) referring to the compressive strength of the material. By decreasing the magnitude of σ_c, the area of stability progressively shrinks, until an ultimate value is identified (at which the area of stability is reduced to a single point). The ratio between the actual compressive strength and the ultimate value thus determined provides the so-called Durand–Claye safety factor [25]. Hence, assuming a very low, fictitious magnitude of σ_c can be useful for defining the safety margin of a masonry structure with respect to the real compressive strength. The achieved funicular polygon of minimum thrust is given in Fig. 5(b). As expected, a flatter solution is found, with an increased horizontal component of the reaction, which is $R_{xh} = 20.09$ kN. Again, two constraints of the type in Eq. (10)-(e) are active at both end joints. With respect to the previous case, a suitable increase in the area of the stress block at the joint is required to provide equilibrium with the axial component of the force in the outer branches of the polygon. Another pair of (symmetrically distributed) constraints according to Eq. (10)-(e) is active at the joints of the keystone, again calling for an area of the stress block that is large enough to avoid crushing.

Then, the case of finite friction is considered by implementing the full statement in Eq. (10). The method outlined in Section 4 is preliminary adopted to detect values of the angle of friction inducing some sliding at incipient collapse. The funicular polygon of minimum thrust for an arch with $\sigma_c = -1000$ MPa and $\tan\psi = 0.0046$ is

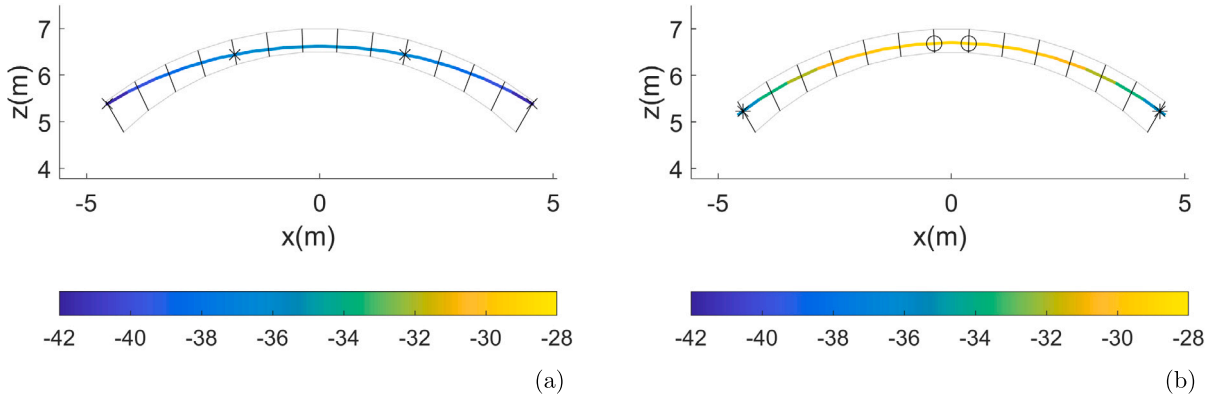

Fig. 6. Funicular polygons of minimum thrust for an arch with finite friction: $\sigma_c = -1000$ MPa and $\tan\psi = 0.0046$ ($R_{xh} = 35.90$ kN) (a); $\sigma_c = -0.15$ MPa and $\tan\psi = 0.1036$ ($R_{xh} = 28.92$ kN) (b). The colours correspond to the value of the forces in the branches (in kN).

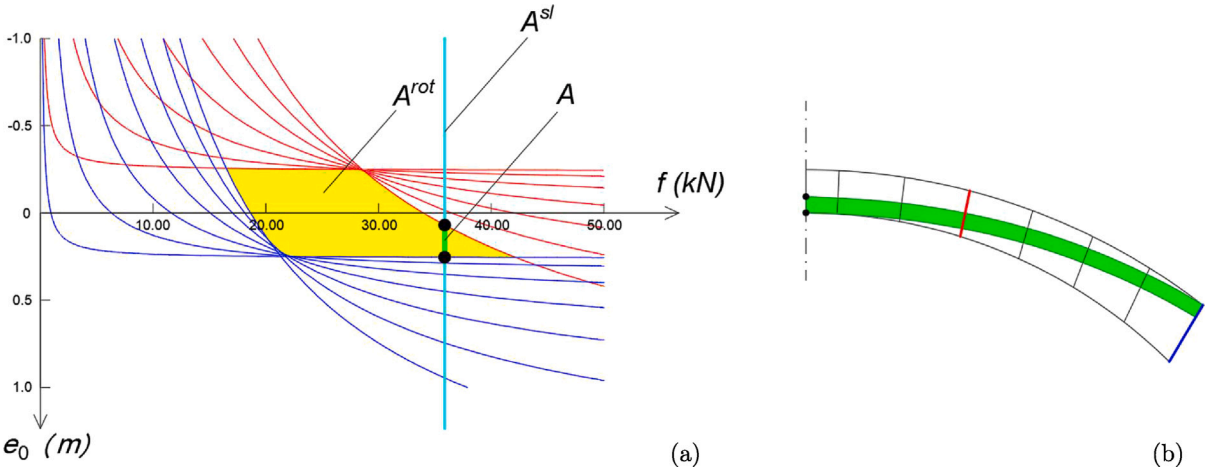

Fig. 7. The stability area method for an arch with $\sigma_c = -1000$ MPa and $\tan\psi = 0.0046$. The stability area is reduced to a green vertical segment (a); the set of corresponding limit thrust lines (b). (For interpretation of the references to colour in this figure legend, the reader is referred to the web version of this article.)

represented in Fig. 6(a). The extremely low value of the friction angle calls for a very flat network, whose branches are almost perpendicular to the joints. Four friction constraints of the type in Eq. (10)-(f) are active. Compared to the case represented in Fig. 5(a), which assumes the same σ_c, the value of the horizontal reaction is more than double ($R_{xh} = 35.90$ kN). Another simulation is performed considering a small value of the compressive strength, i.e. $\sigma_c = -0.15$ MPa, while slightly increasing the friction coefficient, that is $\tan\psi = 0.1036$. The achieved solution is represented in Fig. 6(b). Friction constraints are active at the end joints only, whereas those where the limit bending moment is attained according to Eq. (10)-(e) are active both at the end joints and at the edges of the keystone. With respect to the solution represented in Fig. 6(a), the (slight) increase in the value of $\tan\psi$ allows for a (minor) decrease in the magnitude of the horizontal component of the reaction ($R_{xh} = 28.92$ kN). Also, comparing the solution represented in Fig. 6(b) with that given in Fig. 5(b) for the same value of σ_c, the reversal of the compressive region with respect to the median line of the arch is pointed out.

The results reported in Fig. 6 are in full agreement with the prediction of the Durand–Claye method. More in detail, with reference to Fig. 7(a), for $\tan\psi = 0.0046$ the sliding domain A^{sl} shrinks to the bright blue vertical straight line in the (f, e_0) plane, with $\max_i f_i^{sl-} = \min_i f_i^{sl+} = 35.88$ kN, see Eq. (14). The intersection between this straight line and the rotational domain A^{rot} (the yellow region) identifies the area of stability A, which is reduced to a green vertical segment. Although a single value of the crown thrust is obtained, the stability area thus defined matches a set of infinite solutions defined by 0.0688 m $\leq e_0 \leq$ 0.2541 m. This set corresponds to the green vertical segment in Fig. 7(a), and to the thrust lines contained in the green region of Fig. 7(b). Each of these solutions identifies a limit condition, since the internal reaction at the red and at the blue joint in Fig. 7(b) touches the friction cone defined by the angle ψ. Moreover, the direction of sliding is defined by means of Eq. (14): the arch's portion above the red joint slides outwards, while that comprised between the red and the blue joint slides inwards. It is remarked that the location of the critical joints is the same as found by the proposed approach of funicular analysis, see Fig. 6(a).

As regards the area of stability represented in Fig. 8(a), the sliding domain A^{sl}, which corresponds to the bright blue region in the (f, e_0) plane, has only one point in common with the rotational domain A^{rot} (the yellow region). The coordinates of this point in the (f, e_0) plane are $f = 28.90$ kN, $e_0 = 0.0593$ m, and provide only one statically admissible solution. This is plotted as a green point, at the intersection between: (i) the two bold curves, blue and red, corresponding to the attainment of a negative and a positive limit value of the bending moment, respectively; (ii) the blue vertical straight line, corresponding to $\max_i f_i^{sl-}$. By recalling Eqs. (13) and (14), this solution identifies a limit condition: (i) the negative limit bending moment $-M_{i,\xi}^{lim}$ is attained at the joint near the crown section, see the blue thick curve in Fig. 8(a) and the blue dot in Fig. 8(b); (ii) the positive limit bending moment $+M_{i,\xi}^{lim}$ is attained at the springing joint, see the red thick curve in Fig. 8(a) and the red dot in Fig. 8(b); (iii) the limit condition related to friction arises at the springing joint, see the vertical straight line in Fig. 8(a) and the blue joint in Fig. 8(b). The location of the critical

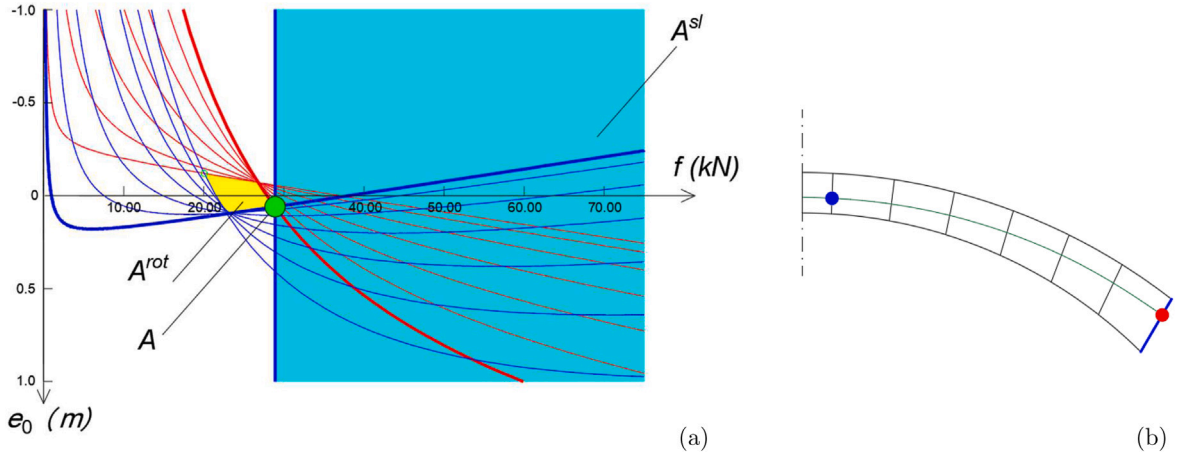

Fig. 8. The stability area method for an arch with $\sigma_c = -0.15$ MPa and $\tan\psi = 0.1036$. The stability area is reduced to a single point (a); the thrust line corresponding to the limit condition thus identified (b).

joints and the value of the crown thrust are in full agreement with those obtained by the proposed approach of funicular analysis, see Fig. 6(b).

It is finally remarked that such very low values of the friction coefficient have been adopted in the presented simulations with the aim of testing the proposed algorithm on two non-trivial cases, both corresponding to degenerated layouts of the stability area, see Figs. 7(a) and 8(a).

5.2. Domes

A dome of revolution, whose reference profile is the same as the arch analysed in the previous section, is addressed. Staggered voussoirs are considered in this investigation, see Section 3.3. Introducing a polar reference system with centre C_{st}, see Fig. 4(a), the sub-blocks are such that each voussoir spans $\Delta\theta = 4.615°$ in terms of polar angle (colatitude) and $\Delta\phi = 15°$ in terms of azimuthal angle. All the parameters defined in the referenced figure take the same values already given in Section 5.1. The keystone consists of a single block with polygonal top and bottom faces.

At first, a network made of meridians only is considered. All the nodes along the perimeter are fully restrained ($n_f = 24$). Each one of the remaining unrestrained nodes ($n = 145$) is loaded by the resultant of the self-weight of the relevant sub-block, or of the voussoir itself (for the keystone). The resultant of the vertical forces reads 637.43 kN. A Gauss–Jordan elimination procedure performed on the system of Eq. (2) allows to conclude that, out of $m = 168$ branches making the meridians, only $m - r = 22$ independent force densities exist (one for each meridian, except two). The number of joints at which strength and friction constraints are enforced equals m. The problem in Eq. (10) was iteratively solved at a first stage, searching for the minimum friction angle for which a statically admissible solution can be found for $\sigma_c = -1000$ MPa. In Fig. 9(a), the funicular network of minimum thrust retrieved for $\tan\psi = 0.1209$ is given, along with the forces in the branches. In this picture and those that follow, only the cross-section of the joints controlled within the optimization procedure are represented (in grey). In each lune, a friction constraint of the type in Eq. (10)-(f) is active at the outer joint. Nearby, a no-tension constraint of the type in Eq. (10)-(h) prevents the vertical coordinate of the vertex of the end voussoir from crossing the extrados. A limited compressive strength/nil tensile strength constraint of the type in Eq. (10)-(e) is active at the joint of the keystone, where the meridian approaches the intrados. Overall, a very flat network is achieved.

As outlined in Section 4, modelling the lunes as independent arches does not always allow for capturing the structural behaviour of the dome. For instance, the activation of the hinges at the keystone cannot occur when such a simplification is dropped. A further investigation is performed searching for funicular networks comprising both meridians and parallels. The number of branches for the full network is $m = 312$, with only $m - r = 28$ independent force densities (one for each parallel, in addition to those already detected in the case of meridians only). The number of joints at which strength and friction constraints are enforced equals 240, which is less than m, due to the staggered arrangement of the voussoirs and the adopted sub-blocking technique. The funicular network of minimum thrust is represented in Fig. 9(b). The only active constraints are those controlling friction at the outer joint. All the parallels are acted upon by compressive forces. This does not affect the magnitude of the horizontal reactions, which are the same as those of the previous solution, but allows decreasing the magnitude of the compressive forces in the central and upper part of the meridians. Indeed, it is remarked that neither limited compressive strength/nil tensile strength constraints nor compression-only enforcements are active at convergence. As already pointed out for the solution represented in Fig. 9(a), a very flat network is retrieved. The active friction constraints force the meridians to lie next to the extrados at the outer joints, while approaching the intrados in the vicinity of the keystone. This layout is not far from the maximum thrust solution that is expected for a dome while considering Heyman's assumptions. In the latter case, the magnitude of the hoop forces is found to increase with increasing polar angle (colatitude), see e.g. the numerical investigations reported in [24], as it can also be observed in Fig. 9(b).

For the validations performed by means of the Durand–Claye method for a single lune, an absolute Cartesian system $(O; x, y, z)$ is chosen, such that the origin O coincides with point C_{st}, while the (x, z) plane belongs to the vertical plane of symmetry of the lune, see Fig. 3(b). The z axis is the axis of revolution of the dome. The generic cross section, i.e. the i-th joint in Fig. 3(b), is schematized as a rectangle of area $l_{i,\eta} \times x_{C_i}\, \Delta\phi$. The area of stability for $\sigma_c = -1000$ MPa and $\tan\psi = 0.1209$ is represented in Fig. 10(a). It coincides with the narrow green region of the (f, e_0) plane, i.e. the intersection between the rotational domain A^{rot} (the yellow region) and the sliding domain A^{sl} (the bright blue region). The area of stability is delimited by the three curves drawn with a thicker stroke and the blue vertical straight line corresponding to $\max_i f_i^{sl-}$. Despite its narrowness, this region identifies a set of infinite admissible thrust lines. Those corresponding to the minimum crown thrust ($f = \max_i f_i^{sl-} = 35.79$ kN) are defined by $0.2117\ \text{m} \le e_0 \le 0.2603$ m, being comprised in the green region plotted in Fig. 10(b). All these thrust lines are characterized by the attainment of the limit condition related to friction at the springing section, see the blue joint in Fig. 10(b). Concerning the thrust lines corresponding to the two extreme values of e_0, the lower thrust line matches the attainment of the negative limit bending moment $-M_{i,\xi}^{lim}$ at the joint near the crown section, see the blue dot in Fig. 10(b). The upper thrust line corresponds to the attainment

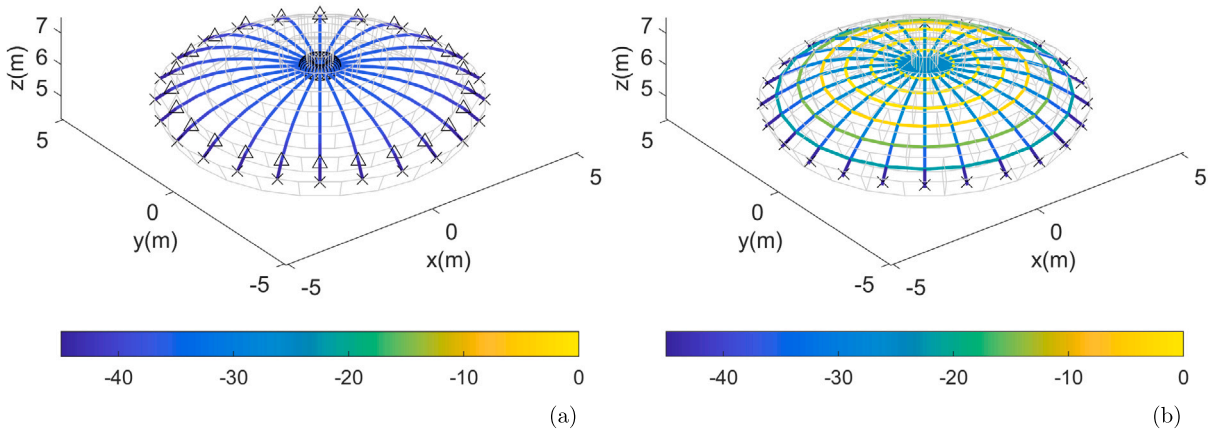

Fig. 9. Funicular networks of minimum thrust for a dome with $\sigma_c = -1000$ MPa and $\tan\psi = 0.1209$: solution with meridians only ($R_h = 35.58$ kN) (a); solution with meridians and parallels ($R_h = 35.58$ kN) (b). The colours correspond to the value of the forces in the branches (in kN).

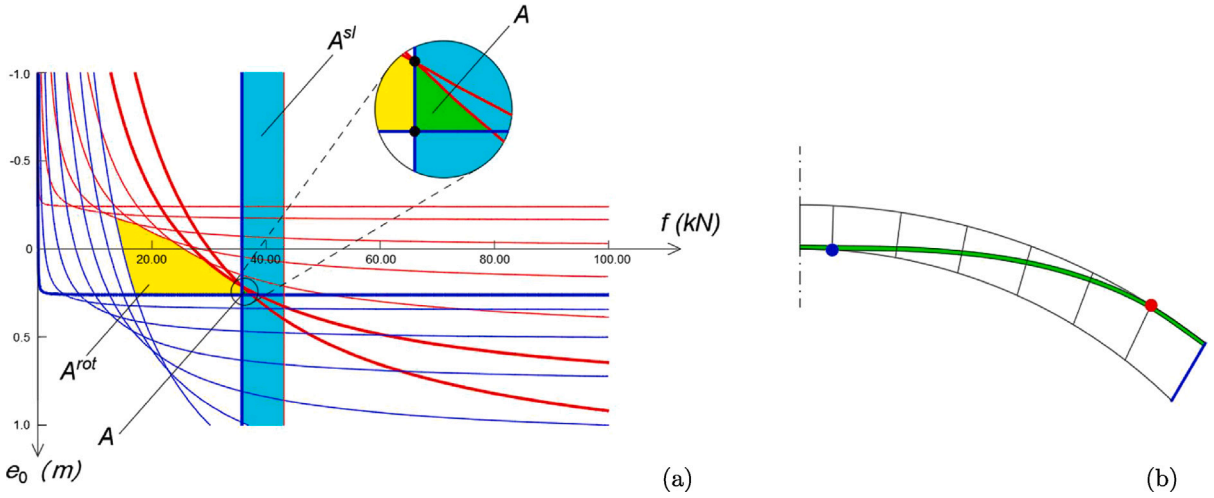

Fig. 10. The stability area method for a dome with $\sigma_c = -1000$ MPa and $\tan\psi = 0.1209$. The stability area (a); the set of thrust lines corresponding to the minimum value of the admissible thrust (b).

of the positive limit bending moment $+M_{i,\xi}^{lim}$ at the joint above the springing section, see the red dot in Fig. 10(b). The location of the critical joints, as well as the value of the minimum thrust, are in good agreement with the results obtained by means of the proposed approach of funicular analysis, see Fig. 9(a). Indeed, it must be remarked that the semi-analytical approach does not control the vertical coordinates of the centroids of the voussoirs, as it is considered in the implemented multi-constrained problem.

A further investigation using the method presented in Section 3 is performed addressing the dome of revolution whose reference profile is depicted in Fig. 4(b). The intrados and the extrados are given by the surface of spheres with centre in $C_{in} = C_{ex} = (0, 0, 0)$ m, and radius $r_{in} = 2.35$ m and $r_{ex} = 2.51$ m, respectively. One half of the angle of embracement reads $\alpha = 80°$. The stereotomy of the staggered voussoirs is defined by radial lines originating from the same point, that is $C_{st} = C_{in} = C_{ex}$. The sub-blocks are such that each block spans $\Delta\theta = 9.41°$ in terms of polar angle (colatitude) and $\Delta\phi = 11.25°$ in terms of azimuthal angle. As before, the keystone consists of a single block with polygonal top and bottom faces. The resultant of the self-weight for the entire dome reads 72.57 kN.

At first, an investigation for a network consisting of meridians only is considered. The minimum friction coefficient for which a statically admissible solution can be retrieved by solving Eq. (10) with $\sigma_c = -0.15$ MPa is $\tan\psi = 0.1242$. The relevant funicular network of minimum thrust is represented in Fig. 11(a). Friction constraints of the type in Eq. (10)-(f) are active at a colatitude equal to 5.5 times $\Delta\theta$. Constraints of the type in Eq. (10)-(e) are active at the joints of the keystone and at a colatitude equal to 7.5 times $\Delta\theta$. No-tension enforcements of the type in Eq. (10)-(h) prevent the vertices at colatitude equal to 3 times $\Delta\theta$ from crossing the upper face of the relevant voussoirs. It is still worth remarking that the activation of the hinges at the keystone is feasible only in case of the assumption of independent lunes. The same dome is further addressed considering both meridians and parallels. The relevant funicular network of minimum thrust is represented in Fig. 11(b). The active constraints are those found in the case of meridians only, except those referring to the joints of the keystone, as expected. Hoop forces arise in the upper part of the dome only. Parallels that lie at colatitude equal to, or greater than, 4 times $\Delta\theta$ are not represented in the picture, being inactive. Indeed, the lower part of the dome behaves as a set of independent lunes, see investigations on the structural behaviour of cracked domes under self-weight [63,64]. Hoop forces are responsible for a decreasing in the meridian forces next to the keystone, with no modification in the magnitude of the horizontal reactions of the solution in Fig. 11(a).

In order to validate the results of the numerical procedure, the Durand–Claye method is applied to the lunes of the dome. It is assumed that $\sigma_c = -0.15$ MPa, whereas the friction coefficient $\tan\psi$ varies. The analysis shows that the rotational domain A^{rot} (the yellow region) is very narrow, near a limit condition related to the single lune, see the stability area in Fig. 12(a), and points a and b in the detail. By assuming

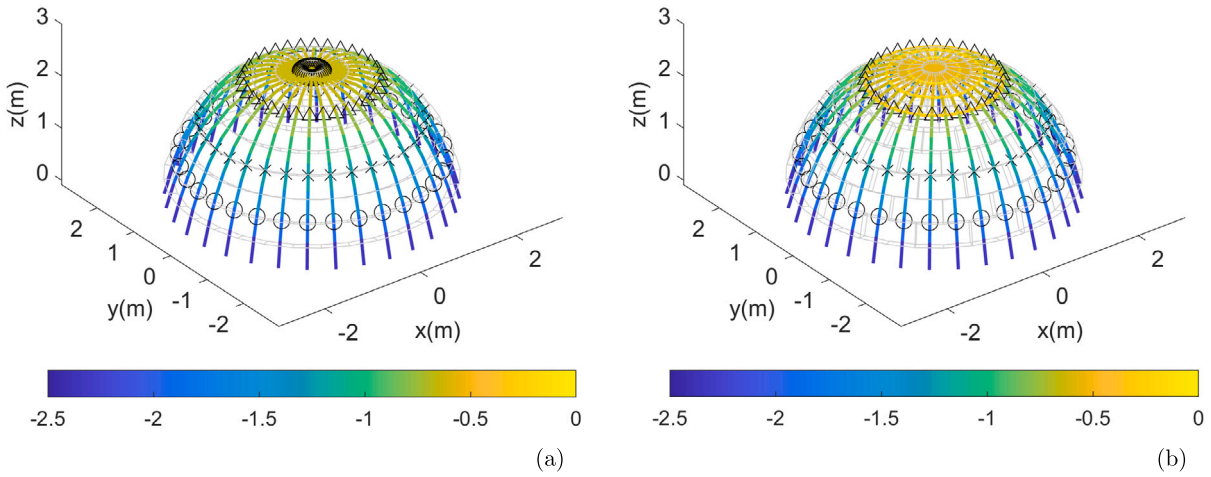

Fig. 11. Funicular networks of minimum thrust for a dome with $\sigma_c = -0.15$ MPa and $\tan\psi = 0.1242$: solution with meridians only ($R_h = 0.633$ kN) (a); solution with meridians and parallels ($R_h = 0.633$ kN) (b). The colours correspond to the value of the forces in the branches (in kN).

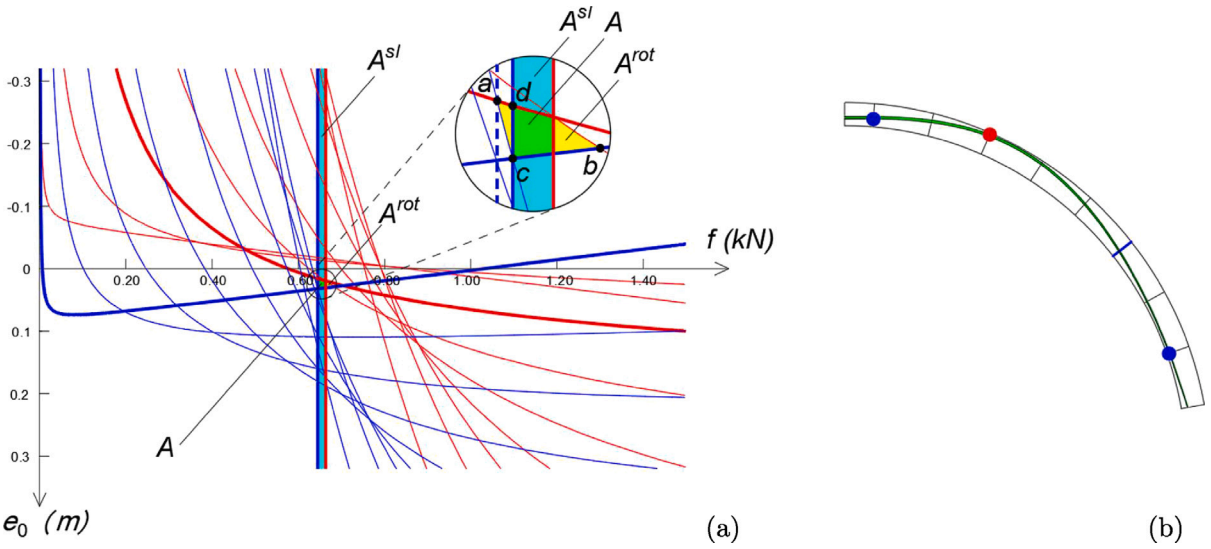

Fig. 12. The stability area method for a dome with $\sigma_c = -0.15$ MPa and $\tan\psi = 0.1211$. The stability area (a); the set of thrust lines corresponding to the minimum value of the admissible thrust (b).

an infinite friction coefficient, the minimum value of the crown thrust is identified by point a ($f = 0.6380$ kN, $e_0 = 0.0145$ m) of the rotational domain, corresponding to the attainment of the limit bending moment at two joints: at a colatitude equal to 2.5 times $\Delta\theta$ (positive limit bending moment $+M^{lim}_{i,\xi}$), and at a colatitude equal to 7.5 times $\Delta\theta$ (negative limit bending moment $-M^{lim}_{i,\xi}$). The dashed blue line in the detail of Fig. 12(a) corresponds to $\max_i f_i^{sl-}$ for $\tan\psi = 0.1260$. It passes through point a, equating the value of the minimum admissible thrust determined above, and identifies a joint subjected to local sliding at a colatitude equal to 5.5 times $\Delta\theta$. By decreasing the friction coefficient, the vertical straight line that corresponds to $f = \max_i f_i^{sl-}$ moves to the right. In particular, for $\tan\psi = 0.1211$, it passes through point c, see the thick blue line in the detail of Fig. 12(a). The area of stability results to be the narrow green region of the (f, e_0) plane, which corresponds to a set of infinite admissible thrust lines. Those characterized by the minimum value of the crown thrust $f = \max_i f_i^{sl-}$ are defined by the vertical segment $c - d$, with $0.0159\ \text{m} \le e_0 \le 0.0323$ m, see Fig. 12(a). The corresponding thrust lines are plotted in Fig. 12(b). All of these solutions match the attainment of the limit condition related to friction at a colatitude equal to 5.5 times $\Delta\theta$. Moreover, the thrust line identified by point c corresponds to the attainment of the negative limit bending moment $-M^{lim}_{i,\xi}$ at two joints: the joint near the crown section, and that identified by a colatitude equal to 7.5 times $\Delta\theta$, see the blue dots in Fig. 12(b). The thrust line related to point d identifies the attainment of the positive limit bending moment $+M^{lim}_{i,\xi}$. This occurs at the joint defined by a co-latitude equal to 2.5 times $\Delta\theta$, see the red dot in Fig. 12(b). Also in this case, a good agreement is observed between the results obtained by means of the two methods.

5.3. Cloister vault

A cloister vault is addressed, which is found by intersection at right angles of two barrel vaults. For both, the reference section is the one represented in Fig. 4(a). The parameters defined in the figure are assumed to take the same value already used to investigate the arch of Section 5.1. This holds for both the geometry of the masonry envelope and the stereotomy aspects, with the only exception that the number of blocks is here set to fourteen. Staggered voussoirs are considered, according to the sub-block modelling approach described in Section 3.3. The same technique is used to address the voussoirs

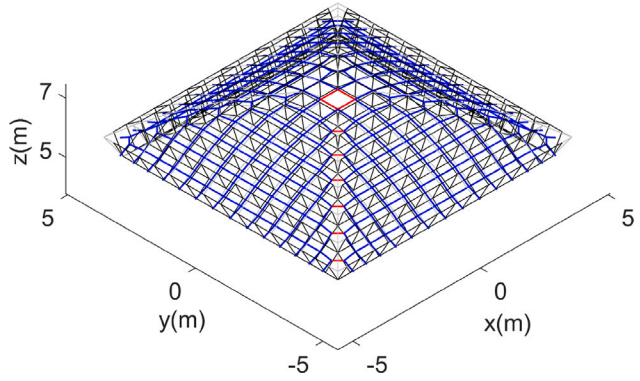

Fig. 13. Geometry and stereotomy of a cloister vault, along with a funicular network of the type implemented in the numerical investigation. Independent branches are marked in red. (For interpretation of the references to colour in this figure legend, the reader is referred to the web version of this article.)

lying at the intersection of the four lunes. Their complex shape is handled by subdividing each voussoir in two symmetric sub-blocks, thus defining two vertices of the network per voussoir. The branch connecting these two vertices inside the corner block is disregarded when enforcing constraints in Eqs. (10)-(e) and (10)-(f), see Fig. 2. In Fig. 13, a funicular network of the type investigated next is depicted, along with the geometry of the entire cloister vault and the stereotomy of the voussoirs. It is remarked that the shape of the resulting grid is not far from that suggested e.g. in [65] to analyse the load path in cloister vaults.

The grid is made of $n_s = 276$ vertices. The nodes lying along the perimeter are fully restrained ($n_f = 56$), whereas the remaining ones are loaded by the self-weight of the relevant sub-blocks. The resultant of the vertical forces reads 821.80 kN. The analysis of the augmented matrix governing the horizontal equilibrium points out that the independent force densities are $m-r = 10$, out of $m = 444$ branches. The independent branches used in the simulation are marked in red in Fig. 13. Hence, the optimization problem of Eq. (10) is set up in terms of a small number of minimization unknowns, which is 66. The number of joints at which strength and friction constraints are enforced is 332.

The first investigation on the equilibrium of the vault is performed considering Heyman's assumptions. The requirement of infinite compressive strength is approximated by using $\sigma_c = -1000$ MPa in Eq. (10)-(e), whereas the constraints in Eq. (10)-(f) are disregarded to deal with infinite friction resistance. The computed funicular network, along with the element forces in its branches, is reported in Fig. 14(a). Limited compressive strength/nil tensile strength constraints of the type in Eq. (10)-(e) are active at the joints all along the perimeter, except for the corner voussoirs, where a limited set of enforcements of the type in Eq. (10)-(g) prevents the arising of tensile stresses in the upper part of the blocks. Local enforcements of the type in Eq. (10)-(f) are active at the crown, preventing the arising of any tensile stress in the lower part of the voussoirs. Indeed, meridians span from the lowest level of the abutments, some of them becoming tangent to the extrados of the vault at the keystone. A remarkable difference in the magnitude of the horizontal reaction exists, when comparing the meridians located in the middle of the lune (where $R_h^{\max} = 17.67$ kN is achieved) and those at the corners (where $R_h^{\min} = 0.25$ kN is found). It is pointed out that parallels are almost inactive in the lower part of the vault.

A further investigation is performed accounting for finite strength and finite friction, assuming $\sigma_c = -0.15$ MPa and $\tan\psi = 0.4$, respectively. The achieved network of minimum thrust is depicted in Fig. 14(b). Its overall shape is characterized by noticeable differences with respect to the network represented in Fig. 14(a). Friction constraints are active for all the joints along the perimeter. A limited number of strength constraints is active at the corner to prevent crushing of the lower part of the voussoirs. A set of constraints of the type in Eq. (10)-(e) is active at some joints around the keystone, either crossed by meridians or parallels, calling for a suitable depth of the stress block to avoid crushing. Because of the friction constraints, a smaller inclination on the horizontal plane is found, with respect to the previous case, in the branches at the base of the vault. This implies an overall increase in terms of resulting horizontal reactions (i.e. the objective function). However, the difference between the maximum value of the horizontal reaction ($R_h^{\max} = 16.81$ kN) and the minimum one ($R_h^{\min} = 3.01$ kN) is less marked, pointing out a more homogeneous response of the meridians. Looking at the parallels, most of them are remarkably more stressed than in the network of Fig. 14(a).

6. Conclusions and ongoing research

A numerical method has been proposed to address the funicular analysis of masonry structures such as arches, domes, and vaults, taking into account stereotomy aspects. The force density method has been employed to handle the equilibrium of the loaded vertices of the funicular network. These lie along vertical lines passing through the centroids of the voussoirs, or of suitable sub-blocks introduced to handle staggered masonry and blocks with complex geometry. For the resulting grid having fixed plan projection, the minimization of the horizontal thrusts has been stated in terms of the height of the restrained nodes and of any set of independent force densities. An optimization problem characterized by a limited number of unknowns has been formulated and solved by means of techniques of sequential convex programming, which can effectively account for multiple sets of local enforcements. These include no-tension constraints for the force densities to achieve anti-funicular networks, and the enforcement of lower and upper bounds for the vertical coordinates of the unrestrained vertices of the network to get compression-only blocks. Local constraints have been introduced at each joint to control the value of the maximum normal stress and the ratio shear to normal component of the force between two adjacent voussoirs. The former prescription calls for a suitable area of the compression-only stress block to avoid crushing. In this regard, a strength criterion for axial loads having eccentricity with components along the principal axes of the cross-section has been implemented. The latter prescription enforces Coulomb's friction law to prevent sliding failure.

The proposed numerical method has been validated against results found through the semi-analytical graphical approach known as the stability area method, considering at first the equilibrium of an arch for different assumptions on the compressive strength and the friction coefficient (see Section 5.1) and, then, the equilibrium of domes of revolutionwith different geometry and stereotomy in meridians-only networks (see Section 5.2). Grids allowing for both meridians and parallels have been investigated, as well, by means of the proposed algorithm. A cloister vault has been analysed to point out peculiar features of the solution attained for finite strength and finite friction with respect to that found under Heyman's assumptions (see Section 5.3).

The proposed method allows generating statically admissible solutions for any given loading scenario. When infinite friction is assumed, with finite either infinite compression strength, the safety of the structure follows. In the case of finite friction, the validity of the solution can be checked, as suggested in the literature, by investigating the possible arising of self-equilibrating stress resultants. No critical issue is reported for the curved structures considered in the numerical studies. This was expected, because of symmetry.

The current research is mainly devoted to the assessment of the proposed method in case of general loading, including the effect of seismic actions. Investigations of networks inspired by load paths retrieved via linear elastic no-tension analyses of vaults, see e.g. [66,67], and testing of grids that are consistent with the expected behaviour of different masonry patterns are ongoing. Special attention will be devoted to

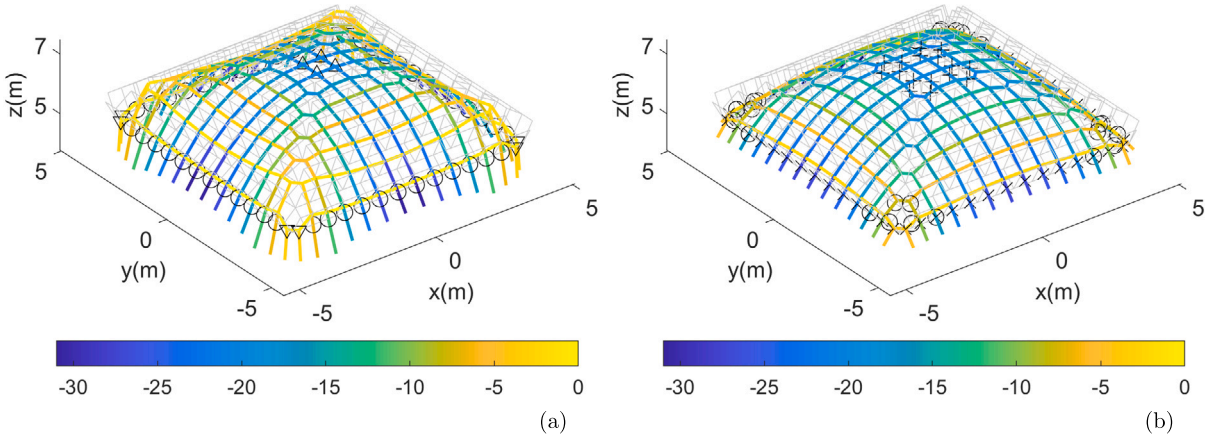

Fig. 14. Funicular networks of minimum thrust for a cloister vault: $\sigma_c = -1000$ MPa and infinite friction ($R_h^{\max} = 17.67$ kN, $R_h^{\min} = 0.25$ kN) (a); $\sigma_c = -0.15$ MPa and $\tan\psi = 0.4$ ($R_h^{\max} = 16.81$ kN, $R_h^{\min} = 3.01$ kN) (b). The colours correspond to the value of the forces in the branches (in kN).

the implementation of general failure criteria at the joint interfaces, and to the validation of the proposed method focusing on structures characterized by challenging equilibrium solutions, see e.g. the case of masonry spiral stairs [68].

CRediT authorship contribution statement

Danila Aita: Conceptualization, Methodology, Data curing, Formal analysis, Writing. **Matteo Bruggi:** Conceptualization, Methodology, Software, Formal analysis, Writing.

Declaration of competing interest

The authors declare that they have no known competing financial interests or personal relationships that could have appeared to influence the work reported in this paper.

Data availability

Data will be made available on request

References

[1] Coulomb CA. Essai sur une application des règles de maximis et minimis à quelques problèmes de statique, relatifs à l'architecture, Mémoires de Mathématique et de Physique. In: Académie Royale des Sciences, Paris. 1776, p. 343–82.
[2] Heyman J. The stone skeleton. Int J Solids Struct 1966;2(2):249–79.
[3] Kooharian A. Limit analysis of voussoir (segmental) and concrete arches. J Am Concr Inst 1952;24(4):317–28.
[4] Alexakis H, Makris N. Limit equilibrium analysis of masonry arches. Arch Appl Mech 2015;85(9–10):1363–81.
[5] Hooke R. A description of helioscopes, and some other instruments. London, UK: John & Martin Printer to the Royal Society; 1675.
[6] Maxwell JC. On reciprocal figures and diagrams of forces. Philos Mag 1864;26:250–61.
[7] Aita D. Revisiting classic methods for the equilibrium analysis of masonry arches and domes. In: Milani G, Sarhosis V, editors. From corbel arches to double curvature vaults: Analysis, conservation and restoration of architectural heritage masonry structures. Springer International Publishing; 2022, p. 123–68.
[8] D'Altri AM, Sarhosis V, Milani G, Rots J, Cattari S, Lagomarsino S, et al. Modeling strategies for the computational analysis of unreinforced masonry structures: Review and classification. Arch Comput Methods Eng 2020;27(4):1153–85.
[9] O'Dwyer D. Funicular analysis of masonry vaults. Comput Struct 1999;73(1–5):187–97.
[10] Block P, Ochsendorf J. Thrust network analysis: A new methodology for three-dimensional equilibrium. J Int Assoc Shell Spat Struct 2007;48(155):167–73.
[11] Marmo F, Rosati L. Reformulation and extension of the thrust network analysis. Comput Struct 2017;182:104–18.
[12] Nodargi NA, Bisegna P. Generalized thrust network analysis for the safety assessment of vaulted masonry structures. Eng Struct 2022;270. 114878.
[13] Schek H. The force density method for form finding and computation of general networks. Comput Methods Appl Mech Engrg 1974;3(1):115–34.
[14] Block P, Lachauer L. Three-dimensional funicular analysis of masonry vaults. Mech Res Commun 2014;56:53–60.
[15] Fraternali F, Angelillo M, Fortunato A. A lumped stress method for plane elastic problems and the discrete-continuum approximation. Int J Solids Struct 2002;39(25):6211–40.
[16] Fraternali F. A thrust network approach to the equilibrium problem of unreinforced masonry vaults via polyhedral stress functions. Mech Res Commun 2010;37(2):198–204.
[17] Fraternali F, Carpentieri G. On the correspondence between 2D force networks and polyhedral stress functions. Int J Space Struct 2014;29(3):145–59.
[18] Angelillo M, Babilio E, Fortunato A. Singular stress fields for masonry-like vaults. Contin Mech Thermodyn 2013;25(2–4):423–41.
[19] Angelillo M, Fortunato A, Montanino A, Lippiello M. Singular stress fields in masonry structures: Derand was right. Meccanica 2014;49(5):1243–62.
[20] Gesualdo A, Cennamo C, Fortunato A, Frunzio G, Monaco M, Angelillo M. Equilibrium formulation of masonry helical stairs. Meccanica 2017;52(8):1963–74.
[21] Fraddosio A, Lepore N, Piccioni MD. Thrust surface method: An innovative approach for the three-dimensional lower bound limit analysis of masonry vaults. Eng Struct 2020;202. 111962.
[22] Fantin M, Ciblac T. Extension of thrust network analysis with joints consideration and new equilibrium states. Int J Space Struct 2016;31(2–4):190–202.
[23] Nodargi NA, Bisegna P. A new computational framework for the minimum thrust analysis of axisymmetric masonry domes. Eng Struct 2021;234. 109846.
[24] Bruggi M. A constrained force density method for the funicular analysis and design of arches, domes and vaults. Int J Solids Struct 2020;193–194:251–69.
[25] Durand-Claye A. Note sur la vérification de la stabilité des voûtes en maçonnerie et sur l'emploi des courbes de pression. Ann Ponts Chaussées 1867;13:63–93.
[26] Aita D, Barsotti R, Bennati S. Equilibrium of pointed, circular, and elliptical masonry arches bearing vertical walls. J Struct Eng 2012;138(7):880–8.
[27] Aita D, Barsotti R, Bennati S. Looking at the collapse modes of circular and pointed masonry arches through the lens of Durand–Claye's stability area method. Arch Appl Mech 2019;89(8):1537–54.
[28] Aita D, Barsotti R, Bennati S. Studying the dome of Pisa cathedral via a modern reinterpretation of Durand–Claye's method. J Mech Mater Struct 2019;14:603–19.
[29] Drucker DC. Limit analysis of two and three dimensional soil mechanics problems. J Mech Phys Solids 1953;1(4):217–26.
[30] Radenkovic D. Théorèmes limites pour un materiau de Coulomb à dilatiation non standardisée. C R Math Acad Sci Paris 1961;252:4103–4.
[31] Palmer AC. A limit theorem for materials with non-associated flow laws. J Mec 1966;5(2):217.
[32] Livesley RK. Limit analysis of structures formed from rigid blocks. Int J Numer Methods Eng 1978;12(12):1853–71.
[33] Boothby TE. Stability of masonry piers and arches including sliding. J Eng Mech 1994;120(2):304–19.
[34] Lo Bianco M, Mazzarella C. Limit load of masonry structures. Venezia, Italy: Final Report IABSE symp; 1983, p. 187–94.
[35] Baggio C, Trovalusci P. Limit analysis for no-tension and frictional three-dimensional discrete systems. Mech Struct Mach 1998;26(3):287–304.
[36] Baggio C, Trovalusci P. Collapse behaviour of three-dimensional brick-block systems using non-linear programming. Struct Eng Mech 2000;10(2):181–95.
[37] Ferris MC, Tin-Loi F. Limit analysis of frictional block assemblies as a mathematical program with complementarity constraints. Int J Mech Sci 2001;43(1):209–24.

[38] Casapulla C. Dry rigid block masonry: Safe solutions in presence of Coulomb friction. WIT Trans Built Environ 2001;55:251–61.
[39] D'Ayala D, Casapulla C. Limit state analysis of hemispherical domes with finite friction. In: Lourenço PB, Roca P, editors. Proceedings of the 3rd international conference structural analysis of historical constructions. 2001, p. 617–26.
[40] Sinopoli A. Unilaterality and dry friction: A geometric formulation for two-dimensional rigid body dynamics. Nonlinear Dyn 1997;12(4):343–66.
[41] Sinopoli A, Corradi M, Foce F. Modern formulation for preelastic theories on masonry arches. Eng Mech 1997;123(3):204–13.
[42] Simon J, Bagi K. Discrete element analysis of the minimum thickness of oval masonry domes. Int J Archit Herit 2016;10(4):457–75.
[43] Beatini V, Royer-Carfagni G, Tasora A. A regularized non-smooth contact dynamics approach for architectural masonry structures. Comput Struct 2017;187:88–100.
[44] Cocchetti G, Rizzi E. Analytical and numerical analysis on the collapse modes of least-thickness circular masonry arches at decreasing friction. Frat Int Strutt 2020;14(51):356–75.
[45] Pepe M, Pingaro M, Trovalusci P. Limit analysis approach for the in-plane collapse of masonry arches. Proc Inst Civ Eng: Eng Comput Mech 2021;174(2):66–81.
[46] Aita D, Sinopoli A. Two different approaches for collapse of nonsymmetric masonry arches: Monasterio's treatment versus limit equilibrium analysis. J Eng Mech 2021;147(10).
[47] Cercadillo-García C, Fernández-Cabo JL. Analytical and numerical funicular analysis by means of the parametric force density method. J Appl Res Technol 2016;14(2):108–24.
[48] Liew A, Pagonakis D, Van Mele T, Block P. Load-path optimisation of funicular networks. Meccanica 2018;53(1–2):279–94.
[49] Liew A, Avelino R, Moosavi V, Van Mele T, Block P. Optimising the load path of compression-only thrust networks through independent sets. Struct Multidiscip Opt 2019;60(1):231–44.
[50] Bruggi M, Lógó BA, Deák Z. Funicular analysis of ribbed masonry vaults: A case study. Int J Archit Herit 2022;16(12):1809–23.
[51] Pellegrino S, Calladine CR. Matrix analysis of statically and kinematically indeterminate frameworks. Int J Solids Struct 1986;22(4):409–28.
[52] Nodargi NA, Bisegna P. Minimum thrust and minimum thickness of spherical masonry domes: A semi-analytical approach. Eur J Mech A Solids 2021;87. 10422.
[53] Orduña A, Lourenço PB. Three-dimensional limit analysis of rigid blocks assemblages. Part I: Torsion failure on frictional interfaces and limit analysis formulation. Int J Solids Struct 2005;42(18–19):5140–60.
[54] Bruggi M, Laghi V, Trombetti T. Stress-based form-finding of gridshells for Wire-and-Arc Additive Manufacturing considering overhang constraints. Eng Struct 2023;279. 115654.
[55] Christensen PW, Klarbring A. An introduction to structural optimization. Solid mechanics and its applications, vol. 153, Dordrecht, Netherlands: Springer; 2008, p. 1–220.
[56] da Silva GA, Aage N, Beck AT, Sigmund O. Three-dimensional manufacturing tolerant topology optimization with hundreds of millions of local stress constraints. Int J Numer Methods Eng 2021;122(2):548–78.
[57] Giraldo-Londoño O, Paulino GH. PolyStress: a Matlab implementation for local stress-constrained topology optimization using the augmented Lagrangian method. Struct Multidiscip Optim 2021;63(4):2065–97.
[58] Jewett JL, Carstensen JV. Experimental investigation of strut-and-tie layouts in deep RC beams designed with hybrid bi-linear topology optimization. Eng Struct 2019;197. 109322.
[59] Dillen W, Lombaert G, Schevenels M. A hybrid gradient-based/metaheuristic method for Eurocode-compliant size, shape and topology optimization of steel structures. Eng Struct 2021;239. 112137.
[60] Svanberg K. The method of moving asymptotes—a new method for structural optimization. Int J Numer Methods Eng 1987;24(2):359–73.
[61] Nguyen CT, Saheya B, Chang Y, Chen J. Unified smoothing functions for absolute value equation associated with second-order cone. Appl Numer Math 2019;135:206–27.
[62] Durand-Claye A. Note sur la vérification de la stabilité des arcs métalliques et sur l'emploi des courbes de pression. Ann Ponts Chaussées 1867;15:109–44.
[63] Heyman J. Equilibrium of shell structures. Oxford, UK: Oxford University Press; 1977.
[64] Huerta S. Mechanics of masonry vaults: The equilibrium approach. In: Lourenço PB, Roca P, editors. Proceedings of historical constructions. 2001, p. 47–70.
[65] Como M. Statics of historic masonry constructions. Solid and structural mechanics, Cham, Swizerland: Springer; 2017.
[66] Angelillo M, Cardamone L, Fortunato A. A numerical model for masonry-like structures. J Mech Mater Struct 2010;5(4):583–615.
[67] Briccola D, Bruggi M. Analysis of 3D linear elastic masonry-like structures through the API of a finite element software. Adv Eng Softw 2019;133:60–75.
[68] Angelillo M, Olivieri C, DeJong MJ. A new equilibrium solution for masonry spiral stairs. Eng Struct 2021;238. 112176.